

# Adsorption and dissociation of $O_2$ at Be(0001): First-principles prediction of an energy barrier on the adiabatic potential energy surface

Ping Zhang, Bo Sun, and Yu Yang

LCP, Institute of Applied Physics and Computational Mathematics,  
P.O. Box 8009, Beijing 100088, People's Republic of China

## Abstract

The adsorption and dissociation of  $O_2$  molecules at the Be(0001) surface is studied by using density-functional theory within the generalized gradient approximation and a supercell approach. The physisorbed and chemisorbed molecular precursor states are identified to be along the parallel and vertical channels, respectively. It is shown that the HH-Z (see the text for definition) channel is the most stable channel for the molecular chemisorption of  $O_2$ . The electronic and magnetic properties of this most stable chemisorbed molecular state are studied, which shows that the electrons transfer forth and back between the spin-resolved antibonding molecular orbitals and the surface Be  $s$  states. A distinct covalent weight in the molecule-metal bond is also shown. The dissociation of  $O_2$  is determined by calculating the adiabatic potential energy surfaces, wherein the T-Y channel is found to be the most stable and favorable for the dissociative adsorption of  $O_2$ . Remarkably, we predict that unlike the other simple  $s$  metal surfaces such as Al(111) and Mg(0001), the adiabatic dissociation process of  $O_2$  at Be(0001) is an activated type with a sizeable energy barrier.

PACS numbers: 68.43.Bc, 82.20.Kh, 82.45.Jn, 34.80.Ht

## I. INTRODUCTION

It is of great scientific importance to understand the behaviors of diatomic molecules at solid surfaces, including their adsorption and dissociation, and corresponding energy barriers during the bond breaking and bond formation at the surfaces [1, 2]. Of all prototypes, the interaction of  $O_2$  molecules with metal surfaces has gained lots of interest for many technologically relevant processes such as heterogeneous catalysis and corrosion [3]. Theoretically, *ab initio* modeling has been successfully used over a wide range to study the adsorption and dissociation of  $O_2$  molecules at transition metal surfaces. By calculating the adiabatic potential energy surface (PES), it has been found that  $O_2$  molecules will spontaneously dissociate while adsorbing at reactive transition metal surfaces like iron (Fe) [4]. For noble transition metals like gold (Au) [5], silver (Ag) [6, 7], platinum (Pt) [5, 8, 9] and Nickel (Ni) [9], the adsorption of  $O_2$  turns out to depend on the ambient temperature. Remarkably, in all above transition metal systems, the concept of adiabatic PES works very well in explaining and predicting a large amount of physical/chemical phenomena during dissociation process of  $O_2$ .

When the attention is focused on the simple sp metals such as Al(111), however, an uncomfortable gap opens between *ab initio* prediction and experimental observation. The most notable is the long-term enigma of low initial sticking probability of thermal  $O_2$  molecules at Al(111), which has been measured by many independent experiments [10, 11] but cannot be reproduced by adiabatic state-of-the-art density functional theory (DFT) calculations [12, 13, 14]. The central problem is that the adiabatic DFT calculations were unable to find any sizeable barriers on the adiabatic PES, whose presence, however, is essential for explanation of the experimental finding. This has led to speculations that nonadiabatic effects may play an important role in the oxygen dissociation process at the Al(111) surface [13, 15, 16, 17, 18, 19, 20]. Recently, a semiquantitative agreement with the experimental data is achieved by nonadiabatically connecting the trajectories of the approaching  $O_2$  molecules to the spin-triplet PES [21]. Until now, however, it still remains unclear how and in what chemical circumstance this spin-selection rule is reasonable, and different opinions exist in literature [22]. For oxygen dissociation at another simple metal, Mg(0001), *first-principles* DFT calculation also shows the lack of a barrier on the adiabatic PES [23], which is in strong disagreement with experimental observation [24, 25] of a low sticking coefficient

of  $O_2$  at Mg(0001). This discrepancy was ascribed, in a similar manner with that in the  $O_2/Al(111)$  system, to nonadiabaticity in the dissociation process of oxygen molecules [23].

Therefore, it becomes clear that the theoretical study of oxygen dissociation at the simple sp metals is still far from maturity. In particular, considering the fact that up to now most of the theoretical results and conclusions are only based on the  $O_2/Al(111)$  and  $O_2/Mg(0001)$  prototypes, workers are thus confronted with an important question: Does it retain necessary or valid for all simple sp metals (at least, for metals with similar elemental valence electrons to Al or Mg) to take into account such nonadiabaticity as spin-selection rule in obtaining an activated PES? Motivated by this question, in this paper we have carried out a systematic *ab initio* investigation of the adsorption and dissociation of oxygen molecules at Be(0001) surface. Beryllium has the same crystal structure and valence electrons as magnesium does. Subsequently, it is attempting for one to derive that the behaviors of oxygen dissociation at Be(0001) are the same as or similar to that at Mg(0001). Our results, however, show that this is not true. The most distinct is that in the present  $O_2/Be(0001)$  system, our calculated adiabatic PES displays sizeable energy barriers along the dissociation paths. This partially but definitely answers the above question. That is, in the DFT calculations of the simple-metal systems, the inclusion of nonadiabatic effects is not always indispensable for the presence of molecular dissociation barrier.

Besides this basic point of interest, our present study is also motivated by the fact that Be has vast technological applications due to its high melting point and low weight. During these applications, surface oxidation as the main kind of corrosion always needs to be prevented. Thus a systematic study on the adsorption and dissociation of  $O_2$  molecules at Be surfaces, i.e., the initial stage during the surface oxidation process, should be done. Moreover, Be is also a getter in experimental nuclear fusion reactors to adsorb residual gases such as  $O_2$  and  $H_2O$  in the plasma vessel, improving the plasma cleanliness [26], which also makes it highly meaningful to study the adsorption and dissociation of  $O_2$  at Be surfaces. At present there are only very few experimental data on the oxidation of Be, reporting that the surface oxidation begins at an oxidation nucleation center, followed by a spreading growth from the center [26, 27, 28, 29], while *ab initio* studies are entirely lacking. This as a whole encourages us to theoretically report a systematic investigation on the  $O_2/Be(0001)$  system. The rest of this paper is organized as follows: In Sec. II the computational method is briefly described. In Sec. III results for the free oxygen molecule, the bulk Be and clean Be(0001) surface are

given. In Sec. IV and Sec. V we present our results for  $O_2$  adsorption and dissociation at Be(0001) surface, respectively. Finally, we close our paper with a summary of our main results.

## II. COMPUTATIONAL METHOD

The density-functional theory (DFT) total energy calculations were carried out using the Vienna ab initio simulation package [30] with the projector-augmented-wave (PAW) pseudopotentials [31] and plane waves [32]. The so-called "repeated slab" geometries were employed [33]. This scheme consists in the construction of a unit cell of an arbitrarily fixed number of atomic layers identical to that of the bulk in the plane of the surface (defining the dimensional cell), but symmetrically terminated by an arbitrarily fixed number of empty layers (the "vacuum") along the direction perpendicular to the surface. In the present study, the clean  $p(2 \times 2)$ -Be(0001) surface was modeled by periodic slabs consisting of nine Be layers separated by a vacuum of 20 Å, which was found to be sufficiently convergent. Oxygen molecules were symmetrically introduced on both sides of the slab. During our calculations, the positions of the outermost three Be layers as well as the  $O_2$  molecules were allowed to relax until the forces on the ions were less than 0.02 eV/Å, while the central three layers of the slab were fixed in their calculated bulk positions. The plane-wave energy cutoff was set 400 eV. After a careful convergence analysis, we used a  $11 \times 11 \times 1$  k-point grid for the  $p(2 \times 2)$  cell with Monkhorst-Pack scheme [34]. Furthermore, the generalized gradient approximation (GGA) of Perdew et al. [35] for the exchange-correlation potential was employed since the GGA results has been previously validated for the bulk Be [36]. A Fermi broadening [37] of 0.1 eV was chosen to smear the occupation of the bands around  $E_F$  by a finite-T Fermi function and extrapolating to  $T = 0$  K.

## III. BULK BE, CLEAN BE (0001) SURFACE, AND FREE OXYGEN MOLECULE

First, the total energy of the bulk hcp Be was calculated to obtain the bulk lattice parameters. The calculated lattice constants are 2.26 and 3.56 Å respectively for  $a$  and  $c$ , according well with experimental values [38] of 2.285 and 3.585 Å. The band structure and orbital-resolved density of states (DOS) of bulk Be is shown in Fig. 1. Typically, the DOS

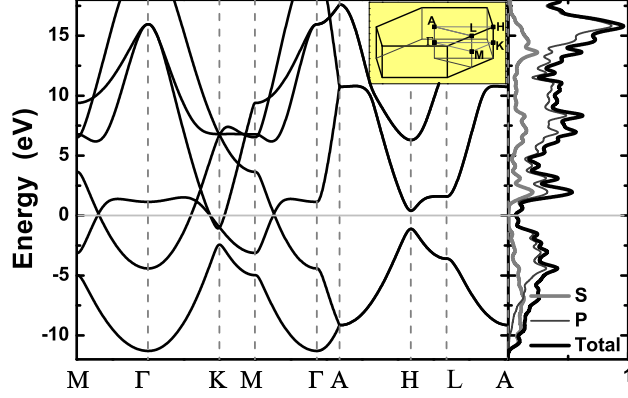


FIG. 1: (Color online). Band structure (left panel) and orbital-resolved DOS (right panel) of the bulk hcp Be. The Fermi energy is set at zero. The inset shows the Brillouin zone.

of bulk Be has a relatively small value at the Fermi energy ( $E_F$ ), because there exists a Dirac point at the Fermi energy in the band structure along the  $\Gamma$ -M direction, and a wide band gap along the  $\Gamma$ -A direction. This anisotropic property of Be differs from that of other alkali-earth metals, whose band structures around the Fermi energy are always nearly free-electrons like. Although the electronic configuration of elemental Be is  $1s^2 2s^2$ , one can see from Fig. 1 that the 2p states play an important role in the DOS behaviors below  $E_F$ , indicating a strong hybridization between s and p electronic states in bulk Be.

The band structure and total DOS for the clean Be(0001) film are shown in Fig. 2. Compared to the bulk case (Fig. 1), one can see from Fig. 2 that there exists no longer Dirac points or band gaps along any direction. Moreover, the DOS at  $E_F$  is prominently enhanced. This result accords well with previous studies [39, 40]. Similar results have also been observed for W (110) and Mo (110) films [41]. From the inset in Fig. 2, we can see that the surface electronic states around  $E_F$  mainly accumulate within the two topmost Be layers. Further detailed wavefunction analysis shows that these states are mainly Be 2p states. Our clean-surface calculation shows that due to this pronounced surface charge redistribution, the two outmost Be(0001) layers relax significantly from the bulk values. The first-second interlayer contraction is 3.8% and the second-third interlayer expansion is nearly 1.2%, which is in agreement with recent first-principles calculations [42] and comparable with experimental measurements [43].

The total energies of the isolated O atom and free  $O_2$  molecule are calculated in an

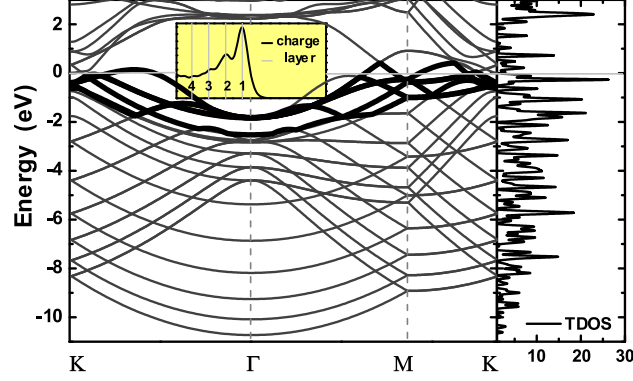


FIG. 2: (Color online). Band structure (left panel) and total DOS (right panel) of the clean  $p(2 \times 2)$  Be(0001) surface with nine atomic layers included in the supercell. The Fermi energy is set at zero. The inset shows the vertical distribution of the charge density close to the surface (Nos. 1-4 enumerate the atomic layers from the surface).

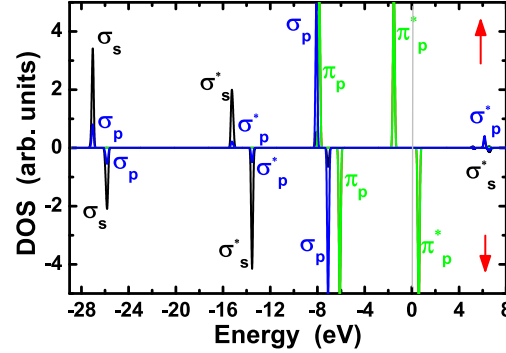


FIG. 3: (Color online). The calculated spin-polarized density of states for the molecular orbitals (MO's) of the free  $O_2$  molecule. The Fermi energy level is set at zero.

orthorhombic cell of scale  $13 \times 11 \times 17 \text{ \AA}^3$  with a  $(3 \times 3 \times 3)$  k-point mesh for the Brillouin zone sampling. The spin-polarization correction has been included. The binding energy of  $O_2$  is calculated to be  $1/2 E_p^{O_2} = 2.89 \text{ eV}$  per atom and the O-O bond length is about  $1.235 \text{ \AA}$ . These results are typical for well-converged DFT-GGA calculations. Compared to the experimental [44] values of  $2.56 \text{ eV}$  and  $1.21 \text{ \AA}$  for O binding energy and bonding length, the usual DFT-GGA result always introduces an overestimation, which reflects the theoretical deficiency for describing the local orbitals of the oxygen.

In order to show the general charge-transfer or redistribution effects on  $O_2$  molecular

orbitals (MO's) after adsorption, here we first calculate and plot in Fig. 3 the MO-resolved local density of states of the free  $O_2$  molecule. Typically, the bonding MO's are lower in energy than the antibonding MO's, for both spins. This ordering of the MO's has important consequences for the molecular bond to the surface. Also it reveals in Fig. 3 that spin splittings are sizeable ( $\sim 2$  eV) for both bonding and antibonding MO's. This reflects Hund's spin rule, which describes ground state as spin-polarized for  $O_2$  ( $S=1$ ). The highest occupied MO (HOMO) and the lowest unoccupied MO (LUMO) are the spin-up and spin-down antibonding MO's, respectively. Our calculated picture of the MO's for a free  $O_2$  molecule is in good agreement with the previous theoretical reports [45, 46].

#### IV. THE ADSORPTION OF $O_2$ MOLECULE

There are four high-symmetry adsorption sites on the Be(0001) surface, including top (T), hcp hollow (HH), fcc hollow (FH), and bridge (B) sites depicted in Fig. 4(a). In this study, we construct twelve initial structures with high symmetries by orienting the  $O_2$  molecule at the four high-symmetry sites respectively along the X (i.e.,  $[1120]$ ), Y (i.e.,  $[1100]$ ) and Z (i.e.,  $[0001]$ ) directions. We also construct several low-symmetry initial structures by rotating the  $O_2$  molecule in the XY, YZ, and XZ planes with small angles. In all the initial configurations, the heights of the  $O_2$  molecules are set at  $h_0 = 4$  Å, see Fig. 3(b). It is found within our expectation that after geometry optimization, these low-symmetry structures will either relax into the high-symmetry ones or be less stable with a lower adsorption energy than the high-symmetry ones. This is similar to what has been observed in studying the adsorption of  $O_2$  molecules at Pb(111) [47]. After geometry optimization, it is found that all the parallel adsorption states with the  $O_2$  molecule lying down on the substrate surface are stable. For the vertical entrances with the  $O_2$  molecule oriented perpendicular to the surface, one exception is the B-Z entrance (namely, the  $O_2$  molecule at the bridge site with the O-O bond along the Z direction), which turns to evolve into the HH-Z adsorption configuration after geometry optimization.

One central quantity tailored for the present study is the average adsorption energy of the adsorbed oxygen species defined as

$$E_{ad} = \frac{1}{N_O} [E_{O_2=Be(0001)} - E_{Be(0001)} - N_O \frac{1}{2} E_{O_2}]; \quad (1)$$

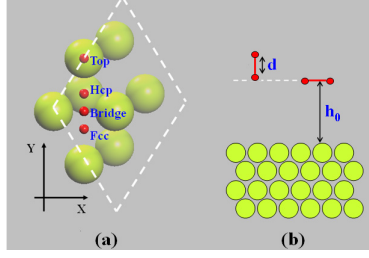


FIG. 4: (Color online) (a) The  $p(2 \times 2)$  surface cell of Be(0001) and four on-surface adsorption sites. Here only the outermost two layers of the surface are shown. (b) The schematic showing that the molecule (with vertical or parallel orientation) is initially away from the surface with a height  $h_0$ . Note that although the atomic radius of O is much larger than that of Be, for convenience in depicting the adsorption positions, here and in the following we use larger circles to denote Be atoms.

where  $N_O$  is the total number of O atoms presented in the supercell,  $E_{O_2=Be(0001)}$ ,  $E_{Be(0001)}$ , and  $E_{O_2}$  are the total energies of the slab containing oxygen, of the corresponding clean Be(0001) slab, and of a free  $O_2$  molecule respectively. According to this definition, a positive value of  $E_{ad}$  indicates that the adsorption is exothermic (stable) with respect to a free  $O_2$  molecule and a negative value indicates endothermic (unstable) reaction.

Starting from the above mentioned entrances and after geometry optimization, the obtained molecular adsorption energy ( $E_{ad}$ ), molecular magnetic moment (MM), work function ( $\phi$ ), adsorption height ( $h$ ), and O-O bond length ( $d$ ) are listed in Table I. From Table I the following molecular adsorption features are revealed: (i) For the  $O_2$  molecule in parallel with Be(0001) surface, the relaxed molecular structures vary very little compared to the initial molecular structures, which suggests the molecular adsorption to be the physisorption in these parallel channels. In these cases, the relaxed adsorption height is around 3.9 Å. The O-O bond length is 1.236 Å, displaying a negligible expansion when compared to that of a free  $O_2$  molecule (1.235 Å). The molecular MM almost saturates at its free value of 2.0  $\mu_B$ , also suggesting the unaltered molecular orbitals in these physisorbed structures. In addition, the work function of the adsorbed Be(0001) surface is almost identical to that of the clean Be(0001) surface, implying negligible charge transfer between the parallel  $O_2$  adsorbate and the surface Be atoms. Finally, the calculated molecular adsorption energy is only -23 meV, which is so small that a little thermal fluctuation may result in desorption



of the  $O_2$  adsorbate with parallel  $O-O$  bond from the  $Be(0001)$  surface. This result is consistent with the recent experimental observation that the reactivity of oxygen atoms with  $Be(0001)$  surface is greater than that of oxygen molecules with  $Be(0001)$  surface [29]. On the other hand, one may question whether, when overcoming the energy barrier by artificially setting the initial molecular distance  $h_0$  to be lower than the above obtained physisorption height ( $\sim 3.9$  Å), new kinds of molecular adsorption state with parallel  $O-O$  bond will occur or not. For this, a large amount of calculations with more lower initial adsorption heights have been carried out and no other parallel molecular physisorption states have been found, for details see discussion in the next section; (ii) For the  $O_2$  adsorbate with the  $O-O$  bond oriented perpendicular to  $Be(0001)$  surface, as shown in Table I, the relaxed molecular structures display a signature of chemisorption. Among them the HH-Z configuration is most stable with the largest molecular adsorption energy of  $\sim 0.5$  eV (per atom). In this channel the adsorption height is decreased to be 1.58 Å, and prominently, the molecular MM is largely decreased to be  $0.8$  Å, which suggests a pronounced charge redistribution among the MO's via interaction with the  $Be(0001)$  surface. The  $O-O$  bond in this most stable chemisorption channel is 1.471 Å, indicating a large expansion from the free  $O_2$  molecule and a fundamental weakening of the molecular bonding. In addition, the work function change is also prominent, implying an observable charge redistribution between the chemisorbed  $O_2$  molecule and the  $Be(0001)$  surface. Meanwhile, during the chemisorption of the  $O_2$  molecule, the  $Be(0001)$  surface is also influenced. Specifically, the three Be atoms around the adsorbed  $O_2$  molecule of the HH-Z entrance are pulled out by about 0.3 Å. Recalling that the bulk BeO has an unusual wurtzite structure, it is within one's expectation that  $O_2$  chemisorption in the HH-Z channel (instead of the FH-Z channel) is most energetically favorable. Our additional calculations of the atomic oxygen adsorption at  $Be(0001)$  also show that the hcp hollow site is most stable for atomic oxygen adsorption.

To clarify the bonding interaction between the chemisorbed  $O_2$  molecule (in the HH-Z channel) and the  $Be(0001)$  surface, we calculate and plot in Fig. 5 (a) the electron-density difference  $\rho(r)$ , which is obtained by subtracting the electron densities of noninteracting component systems,  $\rho_{Be(0001)}(r) + \rho_{O_2}(r)$ , from the density  $\rho_{O_2=Be(0001)}(r)$  of the  $O_2/Be(0001)$  system, while retaining the atomic positions of the component systems at the same location as in  $O_2/Be(0001)$ . A positive  $\rho(r)$  obviously represents charge accumulation, whereas a negative  $\rho(r)$  represents charge depletion. One can see from Fig. 5 (a) (where the contour

TABLE I: The calculated adsorption energy per atom ( $E_{ad}$ ), molecular magnetic moment ( $M$ ), work function ( $\Phi$ ), adsorption height ( $h$ ), and O-O bond length ( $d$ ) for physis- and chemisorptions along different channels.

	Channel	$E_{ad}$ (meV)	$M$ ( $\mu_B$ )	$h$ (Å)	$d$ (Å)	$\Phi$ (eV)
Phys.	T-X	23.6	1.97	3.92	1.236	5.44
	T-Y	23.1	1.95	3.91	1.236	5.44
	B-X	23.9	1.97	3.91	1.236	5.44
	B-Y	22.5	1.97	3.93	1.236	5.46
	HH-X	23.8	1.99	3.91	1.236	5.45
	HH-Y	23.3	2.0	3.9	1.236	5.43
	FH-X	23.7	1.99	3.92	1.236	5.46
	FH-Y	22.6	1.99	3.92	1.236	5.46
Chem.	T-Z	75.2	1.5	2.1	1.272	6.76
	HH-Z	506.1	0.8	1.15	1.471	7.78
	FH-Z	377.6	0.9	1.28	1.436	7.63

spacing is  $0.02e/\text{\AA}^3$ ) that the charge redistribution mainly occurs at the surface and involves the chemisorbed  $O_2$  molecule and the two topmost Be (0001) layers. It is apparent that upon molecular chemisorption, the occupation of the surface and subsurface Be  $sp$  states is decreased, while the occupation of  $O_2$  antibonding MO's is increased, which suggests an electron transfer from the former to the latter. Meanwhile, it reveals in Fig. 5(a) that the occupation of other bonding ( $\sigma$ ,  $\pi$ ) and antibonding MO's ( $\sigma^*$ ,  $\pi^*$ ) is also decreased. The target states for these transferred MO charges are of course again the  $O_2$  antibonding MO's, as shown in Fig. 5(a). A well-known harpooning mechanism is responsible for this inter-MO charge transfer. Prominently, the electron redistribution of the  $O_2$  antibonding MO's is largely asymmetric with respect to the two O atoms. The reason is that the lower O atom in the  $O_2$  molecule is in a complex bonding state. Besides interacting with the upper O atom to form a weakly-bound molecule, this lower O atom also strongly interacts with the surface and subsurface Be atoms via a mixed ionic/covalent bonding mechanism. In particular, it is the strong covalency in the Be-O bond that heavily distorts the charge distribution of the  $O_2$  antibonding MO's. To our knowledge, this strong covalency in the

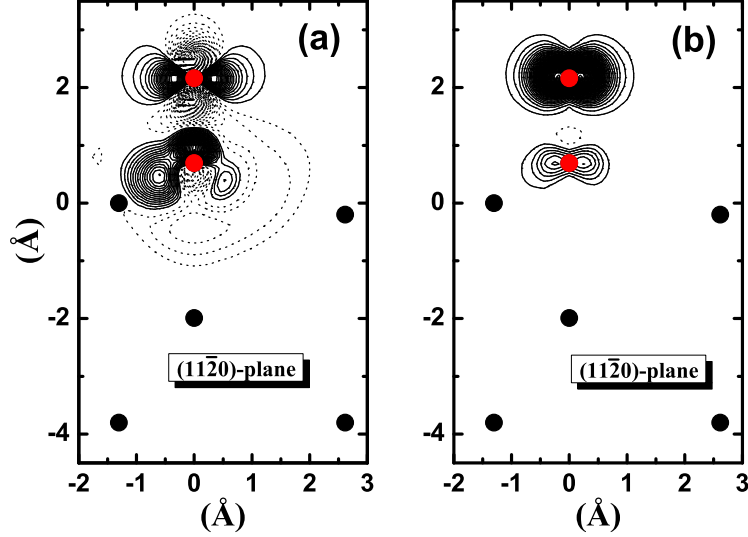


FIG. 5: (Color online) Contour plots of the (a) difference electron density and (b) the spin density for the relaxed  $O_2/Be(0001)$  slab with  $O_2$  molecule chemisorbed along the HH-Z entrance. Solid and dotted lines denote accumulated and depleted densities, respectively.

bond between the metal surface and oxygen molecule has not been theoretically reported in previous studies. On the whole, the charge transfer to the antibonding MO's, as well as the strong covalency in the Be-O bond, weaken the molecular bond and spin polarization. For spin density of the chemisorbed  $O_2$  molecule in the HH-Z channel, see Fig. 5 (b).

In order to gain more insights into the precise nature of the chemisorbed molecular state in the  $O_2/Be(0001)$  system, the orbital-resolved site-projected densities of states (PDOS) for the  $O_2$  molecule (in the most stable HH-Z entrance) and the topmost Be layer are plotted in Fig. 6(a) and 6(b), respectively. By comparison with the case of a free  $O_2$  molecule, one can see that the MO properties of the chemisorbed  $O_2$  in the HH-Z entrance undergo the following fundamental changes: (i) The spin-split PDOS signature (peaks) for the two energy-lowest bonding and antibonding MO's for both spins in Fig. 3 changes to vanish in Fig. 6(a), indicating their breaking in interacting with the Be(0001) surface. This is in accord with the electron-density difference result shown in Fig. 5(a) that charges mostly flow out of these two MO's; (ii) The PDOS peaks for the two nearly-degenerate bonding  $p$  and  $p$  MO's around  $E = -7.5$  eV are broadened upon chemisorption to merge together, with the amplitude becoming much weaker than that in free  $O_2$ . Also, the spin splitting of these two bonding MO's vanishes. These features consistently reveal that although these

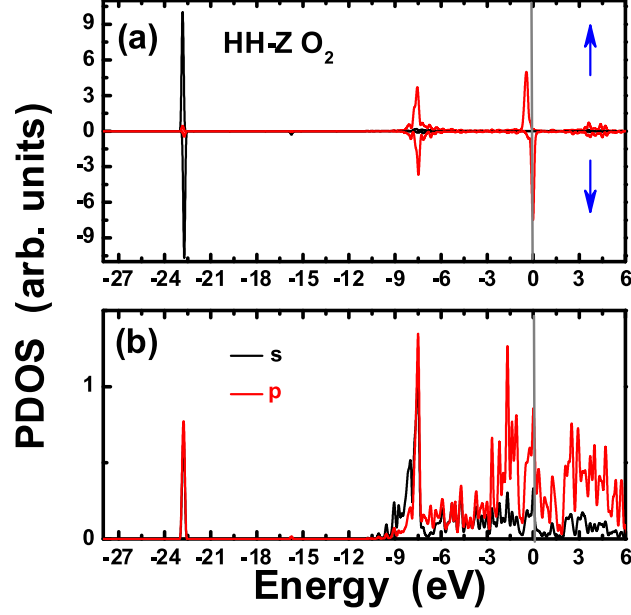


FIG. 6: (Color online) The orbital-resolved PDOS for the chemisorbed O<sub>2</sub> molecule along the HH-Z channel and (b) for the topmost Be layer. The Fermi energy is set at zero. Note that for O<sub>2</sub> the PDOS is plotted in a spin-split form.

two bonding MO's do not lose their nature as the MO's, they are largely reshaped due to their hybridization with the sp orbitals of the surface and subsurface Be atoms. This metal-molecule hybridization is so strong that there develops, as shown in Fig. 6, a sharp sp-hybrid peak around  $E = -7.5$  eV in the PDOS of the topmost Be layer; (iii) The spin-up antibonding  $p$  MO shifts up in energy towards  $E_F$  and is partially depopulated by an observable amount of charges. As a compensation, the spin-down antibonding  $p$  MO shifts down towards  $E_F$  and becomes partially occupied. Obviously, the spin rule prohibits direct charge transfer from the spin-up to spin-down antibonding  $p$  MO. Therefore, the driving or intermediate factor for this charge decrease in the spin-up and increase in the spin-down  $p$  MO's is due to the metallic Be(0001) surface, which accepts electrons from the spin-up  $p$  MO and then donates electrons to the spin-down  $p$  MO. From this aspect, the present result is consistent with the well-known harpooning mechanism, which describes adsorbate-metal interaction by a simultaneous transfer of electrons from the adsorbing molecule into the unoccupied metal states (direct bonding) and a back donation of electrons from occupied metal states into the antibonding adsorbate orbitals. In the present case, this exchange is achieved through

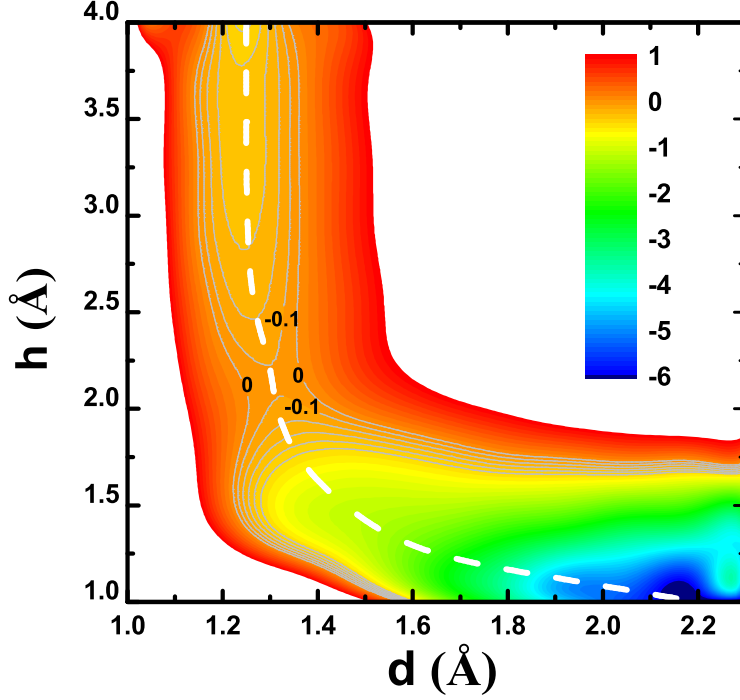


FIG. 7: (Color online) Color filled contour plot of the potential-energy surface for  $O_2$  dissociation at Be(0001) along the T-Y channel, as functions of the  $O_2$  bond length  $d$  and distance  $h$  (from the surface). The contour spacing is 0.1 eV. The dashed line indicates the reaction pathway.

interaction with the  $sp$  orbitals of the Be(0001) surface; (iv) Even more interestingly, to compensate the breaking of the two energy-lowest bonding and antibonding MO's, there develops a new hybrid peak at  $E = -22.7$  eV in the PDOS of the system. From Fig. 6 one can see that this peak is characterized by a strong hybridization of O 2s and Be  $sp$  states.

## V. THE DISSOCIATION OF $O_2$ MOLECULES

In order to deepen our understanding of the initial stage of oxidation at Be(0001) surface from a theoretical point of view, we also calculate the potential energy surfaces (PES's) for  $O_2$  molecules on the Be (0001) surface, which depicts the adiabatic dissociation path with the lowest energy barrier. Since it has been shown that the PES given by the density functional theory gives the result that can be compared with experiments, we expect that our calculated PES provides the qualitative feature of the molecular dissociation process in the present specific  $O_2$ /Be(0001) system. Figure 7 shows the obtained PES as a function of

the distance  $h$  from the surface and the bond length  $d$  of the  $O_2$  molecule along the T-Y channel, which, after a large amount of calculations, turns out to be the most favorable dissociative adsorption channel with largest adsorption energy (4.14 eV/atom) and lowest activation barrier (0.23 eV).

One can clearly see from Fig. 7 the process from initial molecular physisorption with a height of 3.9 Å and bond length of 1.23 Å to the final dissociative adsorption. The most distinct feature in Fig. 7 is that the calculated adiabatic PES exhibits a sizeable energy barrier toward dissociative adsorption. The transition state for this barrier is located at a distance of 2.2 Å from the Be surface, where the O-O bond length is elongated to 1.30 Å. Correspondingly, if we initially put  $O_2$  in the T-Y channel at a height lower than 2.2 Å, then do geometry optimization, the  $O_2$  molecule will spontaneously dissociate with the two O atoms moving to the hcp hollow and fcc hollow sites, respectively. Considering that the previous ab initio calculations have failed to obtain a barrier on the adiabatic PES for oxygen dissociation on the usual simple metals such as Al(111) and Mg(0001), obviously, our present prediction of the activated PES in the  $O_2$ /Be(0001) system is unique. In particular, since beryllium has the same crystal structure and valence electrons as magnesium does, it is attempting to assume that the behavior of oxygen dissociation at Be(0001) is the same as or similar to that at Mg(0001). The result in Fig. 7, however, shows that this intuitive expectation needs to be reshaped.

In the case of Al(111) or Mg(0001), the failure of adiabatic DFT calculations in producing an activated-type PES has been ascribed to the unphysical output that charge transfer occurs even at large molecule-metal distance, which has led to speculations that nonadiabatic effects may play an important role in the oxygen dissociation process at these metal surfaces with the simple sp bands [13, 15, 16, 17, 18, 19, 20, 21, 23]. The unphysical charge transfer at large molecule-metal distance is generally caused by the requirement in the adiabatic description that the electron chemical potential of the  $O_2$  molecule aligns with that of the metal surface in the combined system (metal plus molecule). On the other hand, however, this requirement does not necessarily results in artificial charge transfer between the two largely-separated subsystems. Therefore, there is no universal criterion to judge whether the adiabaticity during molecular dissociation process breaks down or not. The molecule-metal interaction is so species-sensitive that even for the two metals with the same crystal structure and valence electrons, the molecular dissociation process at the surfaces can display

qualitatively different behaviors. To make it more sense, we have carried out a comparative study on the long-distance charge transfer effect by choosing the metal surfaces as Be(0001), Mg(0001), and Al(111). The distances of the  $O_2$  molecule from the three kinds of metal surfaces are fixed at the same value of 7 Å, at which charge transfer should not occur in reality. Also, the  $O_2$  molecules in the three systems are identically chosen to be in the HH-Z entrance. The calculated spin-split PDOS for the  $O_2$  molecule and the charge-density difference  $\rho(r)$  in the three systems are shown in Fig. 8. Clearly, one can see that for  $O_2/Al(111)$  and  $O_2/Mg(0001)$ , although the distance of the  $O_2$  molecule from the surfaces is set to be as large as 7 Å and charge transfer should not be presented in real systems, the adiabatic DFT calculations give yet the contrary results. In these two cases, it reveals in Fig. 8(b) and 8(c) that the LUMO of the ideal  $O_2$  molecule (i.e., the spin-down antibonding  $\pi^*_g$  MO) has shifted down to align with the Fermi energy and becomes partially occupied, accompanying with an observable decreasing of the molecular spin. The O-O bond length also undergoes a little expansion compared to the free value of 1.235 Å. Actually, Fig. 8(b) and 8(c) depict nothing more than what have been known in previous studies, and it is exactly due to this unphysical (metal-molecule or intramolecule) charge transfer that motivates theoretical workers to remedy the calculations by, for example, nonadiabatically constraining the molecular spins. As a direct result, a sizeable energy barrier will appear on the corrected PES [21]. When the attention is paid to the  $O_2/Be(0001)$  system, however, we find that such unphysical large-distance charge transfer effect does not happen in the calculation. In fact, from Fig. 8(a) one can see that at a metal-molecule distance of 7 Å, the calculated spin-split molecular PDOS shows no change with respect to the free case. The LUMO keeps empty and the charge-density difference is zero everywhere. Subsequently, the molecular bond length and spin of  $O_2$  are not influenced at all by the presence of the Be(0001) surface at a distance of 7 Å. Combining with Fig. 7, therefore, we conclude that unlike Al(111) and Mg(0001), the adiabatic DFT calculation presented in this paper is sufficient to predict an activated-type dissociation process of  $O_2$  at Be(0001).

For further illustration of  $O_2$  dissociation at Be(0001), we plot in Fig. 9 four snapshots for the spin density (the contour spacing is  $0.2 \mu_B/\text{Å}^3$ ) evolving along the dissociation path shown in Fig. 7. The values of the corresponding heights  $h$  and relaxed bond lengths  $d$  of the  $O_2$  molecule are also indicated in the figure. One can see from Fig. 9 that as the  $O_2$  molecule approaches the surface along the T-Y channel, the O-O bond length increases,

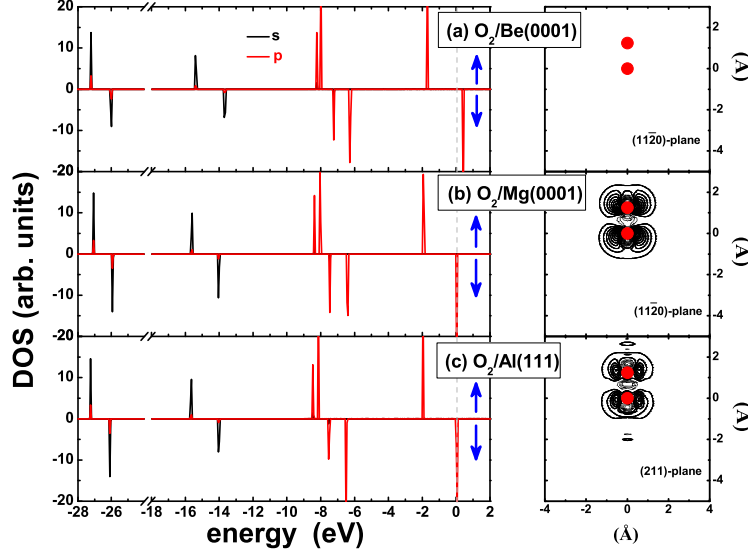


FIG. 8: (Color online) spin-polarized DOS for the molecular orbits of  $O_2$  with a fixed vertical distance of 7 Å from (a) Be(0001), (b) Mg(0001), and (c) Al(111) surfaces. The O-O bond length in each case is allowed to relax. The corresponding charge-density differences ( $r$ ) are plotted on the right side with the contour spacing of  $0.002/\text{Å}^3$ . Solid and dotted lines denote the accumulated and depleted densities, respectively.

while the spin magnetic moment decreases and tends to vanish at  $h = 2.3$  Å. Since there has occurred electron transfer from the substrate to the molecule at this height, thus the disappearance of the spin moment is due to the donation of the minority spins from the substrate not due to the spin flip inside the molecule.

The adiabatic PES's for  $O_2$  dissociation at Be(0001) along the other parallel channels have also been calculated, which are found to have very similar elbow shapes except for visible differences in the transition states and dissociation barriers. To be more clear, a detailed comparison of these PES's is depicted in Fig. 10 by separately plotting the one-dimensional cuts of PES's and O-O bond length as functions of the  $O_2$  height  $h$  from the substrate surface. The insets in each panel in Fig. 10 display the initial and final positions of the two O atoms. Clearly, the dissociative adsorption of  $O_2$  along each of these parallel channels is a direct and activated type. The obtained dissociative adsorption energies, the dissociative energy barriers, and the geometrical parameters for the corresponding transition states, including the height of the  $O_2$  molecule and the O-O bond length, are concluded in



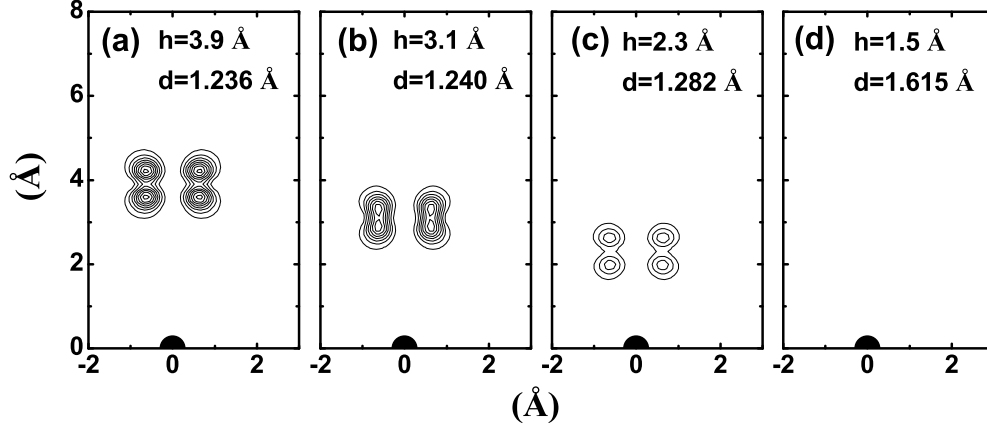


FIG . 9: Snapshots of the spin quenching process during  $O_2$  dissociation at Be(0001) along the T-Y channel. The spacing of the spin-density contours is  $0.2 \mu_B/\text{\AA}^3$ . The corresponding  $O_2$  molecular bond length  $d$  and distance  $h$  from the surface are also indicated.

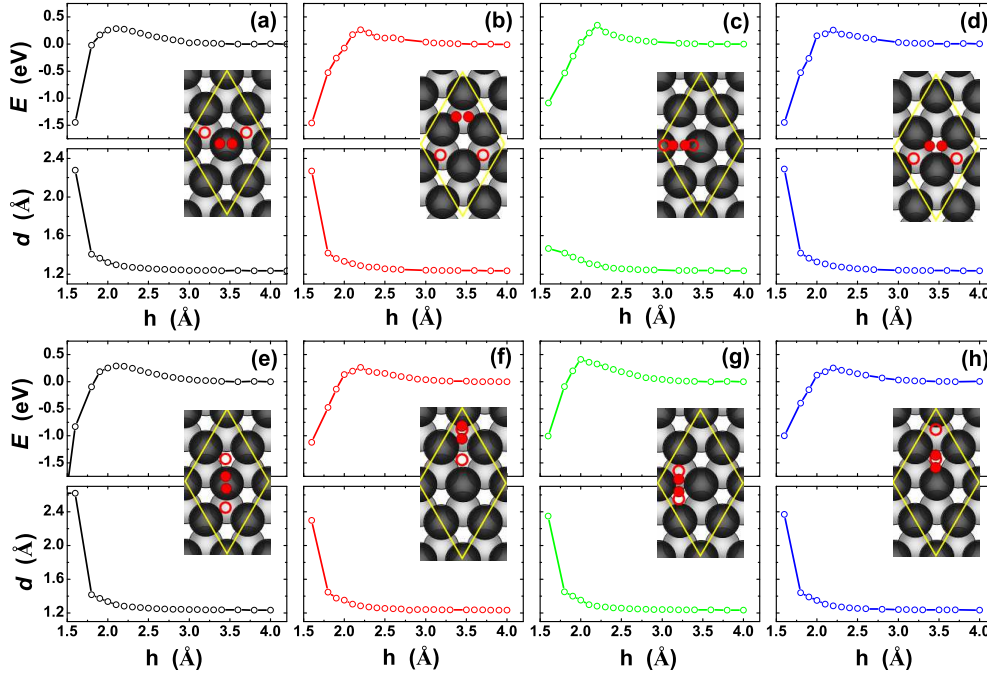


FIG . 10: One-dimensional cuts of the potential-energy surfaces and the corresponding O-O bond lengths as functions of the  $O_2$  distance  $h$  from the surface, for eight different dissociative channels. The inset in each panel indicates the initial (filled circles) and final (hollow circles) atomic positions of  $O_2$ .

TABLE II: The calculated dissociative adsorption energy ( $E_{ad}$ ), dissociative energy barrier ( $E$ ), and geometric parameters (namely, the  $O_2$  molecular bond length  $d$  and distance  $h$  from the surface) of the transition state, along the eight different dissociation channels.

Channel	$E_{ad}$	$E$	$h$ (TS)	$d_{O-O}$ (TS)
T-X	4.00	0.28	2.10	1.30
T-Y	4.14	0.23	2.10	1.30
B-X	3.99	0.26	2.20	1.29
B-Y	4.10	0.26	2.20	1.29
HH-X	3.81	0.35	2.20	1.30
HH-Y	4.09	0.41	2.10	1.30
FH-X	4.00	0.25	2.20	1.29
FH-Y	4.10	0.25	2.20	1.28

Table II. It is found that the dissociation path with both the lowest energy barrier and the largest dissociative adsorption energy is along the T-Y channel. For all the dissociation paths, the O-O bond lengths at the transition states are similar, ranging from 1.28 to 1.30 Å, elongated from the 1.236 Å in an isolated  $O_2$  molecule. Note that no dissociative adsorptions are found for the  $O_2$  molecules along the vertical entrances, which thus are not plotted in Fig. 9 and listed in Table II. This is different from the  $O_2/Al(111)$  system, in which the molecular dissociation along the vertical channels has been predicted to occur as well [12].

## VI. CONCLUSION

In summary, by performing ab initio simulations we have for the first time systematically investigated the adsorption and dissociation of oxygen molecules on the Be(0001) surface. We have identified both the physisorbed and the chemisorbed molecular states, which directly occur along the parallel and vertical channels, respectively. For the most stable chemisorbed molecular state (which is along the HH-Z entrance), in particular, we have studied its electronic and magnetic properties by calculating the charge-density difference, the spin density, and the PDOS, which clearly show the charge transfer from the spin-up

MO to the substrate followed by the back donation from the substrate to the spin-down

$\text{MO}$ , as well as the distinct covalent weight in the chemical bonding between  $\text{O}_2$  and  $\text{Be}(0001)$ . This important covalent weight in the molecule-metal bond has been revealed through the combining fact: (i) The charge is largely accumulated along the  $\text{Be-O}$  bond [Fig. 5(a)]; (ii) The  $\text{O}$ ,  $\text{O}_2$ , and  $\text{MO}$ 's are heavily hybridized with the  $\text{Be}$   $\text{sp}$  states (Fig. 6); (iii) The chemisorbed molecular state in the  $\text{HH-Z}$  channel is much stable than that in the  $\text{FH-Z}$  channel, implying an observable role played by the subsurface  $\text{Be}$  atom beneath the  $\text{O}_2$  molecule.

The energy path for the dissociation of  $\text{O}_2$  on  $\text{Be}(0001)$  surface has been determined by calculating the adiabatic PES's along various channels, among which the  $\text{T-Y}$  channel has been found to be the most stable and favorable for the dissociative adsorption of  $\text{O}_2$ . Remarkably, our results have shown that the adiabatic dissociation process in the present  $\text{O}_2/\text{Be}(0001)$  system is an activated type, with the lowest energy barrier of 0.23 eV in the most stable  $\text{T-Y}$  channel. To our knowledge, this is the first time to theoretically predict a sizeable adiabatic energy barrier during dissociation of  $\text{O}_2$  at the metal surfaces with simple  $\text{sp}$  bands. Thus as a final concluding remark, here we point out that in spite of any previous revealing and specific studies, an in-depth and primary insight into the common nature of the  $\text{O}_2$  dissociation at various simple  $\text{sp}$  metal surfaces remains yet to be attainable.

#### Acknowledgments

This work was supported by the NSFC under grants No. 10604010 and No. 60776063, and by the National Basic Research Program of China (973 Program) under grant No. 2009CB929103.

- 
- [1] G. Darling and S. Holloway, *Rep. Prog. Phys.* 58, 1595 (1995).
  - [2] *The Chemical Physics of Solid Surfaces and Heterogeneous Catalysis*, edited by D. A. King and D. P. Woodruff (Elsevier, Amsterdam, 1988).
  - [3] H. H. Kung, *Transition Metal Oxides, Surface Chemistry and Catalysis* (Elsevier, Amsterdam, 1989); V. E. Henrich and P. A. Cox, *The Surface Science of Metal Oxides* (Cambridge University Press, Cambridge, 1994).
  - [4] P. Blonski, A. Kiejna and J. Hafner, *Phys. Rev. B* 77, 155424 (2008).

- [5] S. Yotsuhashi, Y. Yamada, T. Kishi, W. A. D'Amore, H. Nakanishi and H. Kasai, Phys. Rev. B 77, 115413 (2008).
- [6] H. Nakatsuji and H. Nakai, J. Chem. Phys. 98, 2423 (1993).
- [7] P. A. G. Ravil, D. M. Bird, and J. A. White, Phys. Rev. Lett. 77, 3933 (1996).
- [8] A. Eichler and J. Hafner, Phys. Rev. Lett. 79, 4481 (1997).
- [9] A. Eichler, F. Mittendorfer, and J. Hafner, Phys. Rev. B 62, 4744 (2000).
- [10] H. Brune, J. Wintterlin, J. Trost, G. Ertl, J. Wiechers and R. J. Behm, J. Chem. Phys. 99, 2128 (1993).
- [11] L. Osterlund, I. Zoric, and B. Kasemo, Phys. Rev. B 55, 15452 (1997).
- [12] T. Sasaki and T. Ohno, Phys. Rev. B 60, 7824 (1999); K. Honkala and K. Laasonen, Phys. Rev. Lett. 84, 705 (2000).
- [13] Y. Yourdshahyan, B. Razaznejad, and B. I. Lundqvist, Solid State Commun. 117, 531 (2001).
- [14] Y. Yourdshahyan, B. Razaznejad, and B. I. Lundqvist, Phys. Rev. B 65, 075416 (2002).
- [15] B. Kasemo, Phys. Rev. Lett. 32, 1114 (1974).
- [16] B. Kasemo, R. Toemqvist, J. K. Nørskov, and B. I. Lundqvist, Surf. Sci. 89, 554 (1979).
- [17] G. Katz, Y. Zeiri, and R. Koslo, J. Chem. Phys. 120, 3931 (2004).
- [18] A. M. Wodtke, J. C. Tully, and D. J. Auerbach, Int. Rev. Phys. Chem. 23, 513 (2004).
- [19] A. Hellman, B. Razaznejad, Y. Yourdshahyan, H. Temow, I. Zoric, and B. I. Lundqvist, Surf. Sci. 532-535, 126 (2003).
- [20] A. Hellman, B. Razaznejad, and B. I. Lundqvist, Phys. Rev. B 71, 205424 (2005).
- [21] J. Behler, B. Delley, S. Lorenz, K. Reuter, and M. Scheer, Phys. Rev. Lett. 94, 036104 (2005); J. Behler, K. Reuter, and M. Scheer, Phys. Rev. B 77, 115421 (2008).
- [22] X. L. Fan, W. M. Lau, and Z. F. Liu, Phys. Rev. Lett. 96, 079801 (2006).
- [23] A. Hellman, Phys. Rev. B 72, 201403(R) (2005).
- [24] S. M. Driver, J. Ludecke, G. J. Jackson, and D. P. Woodruff, J. Electron Spectrosc. Relat. Phenom. 99, 235 (1999).
- [25] L. Aballe, A. Barinov, A. Locatelli, S. Heun, and M. Kiskinova, Phys. Rev. Lett. 93, 196103 (2004).
- [26] S. Zalkind, M. Polak and N. Shamir Surf. Sci. 385, 318 (1997).
- [27] S. Zalkind, M. Polak, and N. Shamir, Surf. Sci. 513, 501 (2002).
- [28] S. Zalkind, M. Polak and N. Shamir, Phys. Rev. B 71, 125413 (2005).

- [29] C. Linsmeiser and J. Wanner Surf. Sci. 454, 305 (2000).
- [30] G. Kresse and J. Hafner, Phys. Rev. B 47, 558 (1993); G. Kresse and J. Furthmüller, Comput. Mater. Sci. 6, 15 (1996); G. Kresse and J. Furthmüller, Phys. Rev. B 54, 11169 (1996).
- [31] G. Kresse and D. Joubert, Phys. Rev. B 59, 1758 (1999).
- [32] M. Bockstedte, A. Kley, J. Neugebauer, and M. Scheer, Comput. Phys. Commun. 107, 187 (1997).
- [33] Principles of Surface Physics, edited by F. Bechstedt (Springer, Verlag Berlin Heidelberg, 2003).
- [34] H. J. Monkhorst and J. D. Pack, Phys. Rev. B 13, 5188 (1976).
- [35] J. P. Perdew et al., Phys. Rev. B 46, 6671 (1992).
- [36] E. Wachowicz and A. Kiejna, J. Phys.: Condens. Matter 13, 10767 (2001).
- [37] M. Weinert and J. W. Davenport, Phys. Rev. B 45, 13709 (1992).
- [38] V. M. Amonenko, V. Ye. Ivanov, G. F. Tikhinskiy, and V. A. Finkel, Phys. Met. Metallogr. 14, 47 (1962).
- [39] E. V. Chulkov, V. M. Silkin, and E. N. Shiryakov, Surf. Sci. 188, 278 (1987); P. Hofmann, R. Stumpf, V. M. Silkin, E. V. Chulkov, and E. W. Plummer, *ibid*: 355, L278 (1996).
- [40] J. C. Boettger and S. B. Trickey Phys. Rev. B 34, 3604 (1986).
- [41] E. Rotenberg, J. Schaefer, and S. D. Kevan, Phys. Rev. Lett. 84, 2925 (2000).
- [42] M. Lazzeri and S. de Gironcoli Phys. Rev. Lett. 81, 2096 (1998).
- [43] K. Pohl, J.-H. Cho, K. Terakura, M. Scheer, and E. W. Plummer, Phys. Rev. Lett. 80, 2853 (1998); H. L. Davis, J. B. Hannon, K. B. Ray, and E. W. Plummer, *ibid*: 68, 2632 (1992).
- [44] K. P. Huber and G. Herzberg, Molecular Spectra and Molecular Structure IV: Constants of Diatomic Molecules (Van Nostrand Reinhold, New York, 1979).
- [45] A. Eichler, F. Mittendorfer, and J. Hafner Phys. Rev. B 62, 4744 (2000).
- [46] A. Hellman, B. Razaznejad, and B. I. Lundqvist Phys. Rev. B 71, 205424 (2005).
- [47] Y. Yang, G. Zhou, J. Wu, W. H. Duan, Q. K. Xue, B. L. Gu, P. Jiang, X. C. Ma, and S. B. Zhang, J. Chem. Phys. 128, 164705 (2008).